



HAL
open science

Gas-phase ozonolysis of trans-2-hexenal: Kinetics, products, mechanism and SOA formation

Asma Grira, Carmen Kalalian, J.N. Illmann, I. Patroescu-Klotz, G. El Dib, P. Coddeville, André Canosa, P. Wiesen, Estelle Roth, Abdelkhaleq Chakir, et al.

► **To cite this version:**

Asma Grira, Carmen Kalalian, J.N. Illmann, I. Patroescu-Klotz, G. El Dib, et al.. Gas-phase ozonolysis of trans-2-hexenal: Kinetics, products, mechanism and SOA formation. *Atmospheric Environment*, 2021, 253, pp.118344. 10.1016/j.atmosenv.2021.118344 . hal-03225394

HAL Id: hal-03225394

<https://hal.science/hal-03225394v1>

Submitted on 19 May 2021

HAL is a multi-disciplinary open access archive for the deposit and dissemination of scientific research documents, whether they are published or not. The documents may come from teaching and research institutions in France or abroad, or from public or private research centers.

L'archive ouverte pluridisciplinaire **HAL**, est destinée au dépôt et à la diffusion de documents scientifiques de niveau recherche, publiés ou non, émanant des établissements d'enseignement et de recherche français ou étrangers, des laboratoires publics ou privés.

1 **Gas-phase ozonolysis of trans-2-hexenal: Kinetics,**
2 **products, mechanism and SOA formation**

3
4 **A. Grira^{1,2}, C. Kalalian³, J.N. Illmann⁴, I. Patroescu-Klotz⁴, G. El Dib², P. Coddeville¹,**
5 **A. Canosa², C. Coeur⁵, P. Wiesen⁴, E. Roth³, A. Chakir³, A. Tomas^{1,*}**

6
7 ¹*IMT Lille Douai, Institut Mines-Télécom, Univ. Lille, Centre for Energy and Environment, 59000*
8 *Lille, France*

9 ²*Univ Rennes, CNRS, IPR (Institut de Physique de Rennes) -UMR 6251, F-35000 Rennes, France*

10 ³*Groupe de Spectrométrie Moléculaire et Atmosphérique (GSMA), UMR CNRS 7331, Université de*
11 *Reims, F-51687 Reims, France*

12 ⁴*Institute for Atmospheric and Environmental Research, University of Wuppertal, Germany*

13 ⁵*Laboratoire de Physico-Chimie de l'Atmosphère (LPCA) EA 4493, Université Littoral Côte d'Opale,*
14 *59140 Dunkerque, France*

15
16
17 * Corresponding author: alexandre.tomas@imt-lille-douai.fr

18
19
20 **Submitted to Atmospheric Environment**

21
22
23
24 **Keywords:** aldehyde; ozone; atmosphere; aerosol; kinetics

Credit author statement

AG, CK, JNI, IPK and AT did the experiments.

All authors contribute to the manuscript.

Journal Pre-proof

27 **ABSTRACT**

28 In this work, kinetics, product formation, chemical mechanism and SOA formation for the
29 gas-phase reaction of trans-2-hexenal (T2H) with O₃ are examined using four complementary
30 experimental setups at 298±2 K and atmospheric pressure. Product studies were conducted in
31 two contrasted experimental conditions, with and without OH radical scavenger. The
32 ozonolysis rate constant was determined in both static and dynamic reactors. An average
33 reaction rate constant of $(1.52 \pm 0.19) \times 10^{-18} \text{ cm}^3 \text{ molecule}^{-1} \text{ s}^{-1}$ was determined. Glyoxal and
34 butanal were identified as main products with molar yields of 59±15% and 36±9%,
35 respectively, in the presence of an OH scavenger. Slightly lower values were obtained in the
36 absence of scavenger. Acetaldehyde, propanal and 2-hydroxybutanal were also identified and
37 quantified. A reaction mechanism was proposed based on the observed products. SOA
38 formation was observed with aerosol mass yields > 13% for SOA masses of 400 μg m⁻³. This
39 work demonstrates for the first time that 2-alkenals ozonolysis can be a source of SOA in the
40 atmosphere.

41

42 **1. INTRODUCTION**

43 It is now recognized that biogenic volatile organic compounds (BVOCs) play a major role in
 44 the chemistry of the troposphere from the local to the global scale^[1]. Many BVOCs possess an
 45 unsaturated C=C double bond, which confers them a high reactivity towards the atmospheric
 46 oxidants^[2]. Therefore, these biogenic species largely contribute to the formation of
 47 photochemical smog and tropospheric ozone on one hand and to the budget of hydroxyl
 48 radicals (OH) and the formation of secondary pollutants in the atmosphere on the other
 49 hand^[2]. In addition, the oxidation of biogenic compounds yields less volatile species which
 50 could be a source of biogenic secondary organic aerosols (SOA)^[3,4], one of the most uncertain
 51 factors in the global radiation budget^[5].

52 While current research still focuses on the oxidation of the most abundant biogenic
 53 compounds in the atmosphere like isoprene and limonene^[6,7], a number of unsaturated
 54 oxygenated compounds (aldehydes, ketones and alcohols) have been shown to be
 55 ubiquitously emitted by vegetation^[1,8], especially when plants are damaged by biotic and/or
 56 abiotic stresses^[9-11]. The emission of these species, so-called Green Leaf Volatiles (GLV),
 57 may have significant impacts on the environment and the air quality due to their high
 58 reactivity towards OH, O₃ and NO₃^[9,12,13].

59 *Trans-2-hexenal (T2H)* is a GLV emitted from several different plants^[14], green residues like
 60 oak and pine mulch^[15] and leaf drying^[16]. Once in the atmosphere, T2H can be removed by
 61 reaction with tropospheric oxidants such as OH^[17-19] and NO₃ radicals^[20], Cl atoms^[21] and O₃
 62 ^[20,22,23]. The reaction of T2H with O₃ proceeds as follows:



65 The rate constant was first determined by Atkinson et al.^[20] at ambient temperature using the
 66 relative method. The significant error associated with their determination ($(2 \pm 1) \times 10^{-18} \text{ cm}^3$
 67 $\text{molecule}^{-1} \text{ s}^{-1}$) was assigned to a low consumption of T2H by O₃. An OH radical formation
 68 yield of ~0.62 was also estimated. However, the authors noted that there is a high degree of
 69 uncertainty in their determination. Grosjean et al.^[23] conducted an extensive study and
 70 reported a rate constant $((1.28 \pm 0.28) \times 10^{-18} \text{ cm}^3 \text{ molecule}^{-1} \text{ s}^{-1}$ at 288 K) using an absolute
 71 method with T2H in excess over O₃. Both rate constants determined by Atkinson et al.^[20] and
 72 Grosjean et al.^[23] agree within the uncertainties. A range of carbonyl products was also
 73 observed in Grosjean's study^[23] and their formation yields were calculated towards O₃
 74 consumption. More recently, Kalalian et al.^[22] investigated the kinetics of this reaction at 298

75 K using the absolute method with O₃ in excess over T2H. A consistent rate constant of
76 $(1.37 \pm 0.03) \times 10^{-18} \text{ cm}^3 \text{ molecule}^{-1} \text{ s}^{-1}$ was obtained. Apart from Grosjean et al.^[23], no literature
77 data are available on T2H + O₃ reaction products.

78 Regarding OH + T2H reaction, the three most recent kinetics studies^[17-19] displayed
79 consistent rate constant values, yielding an average OH rate constant of $4.24 \times 10^{-11} \text{ cm}^3$
80 $\text{molecule}^{-1} \text{ s}^{-1}$ at 298 K. NO₃ kinetics was investigated by Atkinson et al.^[20] who determined a
81 rate constant of $1.21 \times 10^{-14} \text{ cm}^3 \text{ molecule}^{-1} \text{ s}^{-1}$ at 298 K. Thus, OH- and NO₃-initiated reactions
82 represent the main removal of T2H in the atmosphere, with lifetimes of 6h and 8h,
83 respectively, while O₃ reaction may only be competitive in polluted areas where high levels of
84 ozone may be found^[24]. Regarding the relevance of T2H atmospheric photolysis, Kalalian et
85 al.^[24] calculated an upper limit of 29 min assuming a quantum yield of 1, while O'Connor et
86 al.^[25] and Jiménez et al.^[18] suggested that T2H photolysis constitutes a negligible pathway
87 compared to its removal through tropospheric oxidants.

88 While these studies focused on the kinetics of these reactions, limited data exist concerning
89 reaction products, with no data on the potential SOA formation in the troposphere. The main
90 objective of the present study was to investigate thoroughly the reaction of T2H with ozone
91 using several complementary experimental setups to improve our knowledge on T2H
92 oxidation by O₃ in the atmosphere. The rate constant was measured with the absolute-rate
93 method in both batch and flow reactors, aiming at enriching our knowledge on the kinetics of
94 the studied reaction. Reaction products were identified with two techniques: Fourier
95 Transform InfraRed (FTIR) spectroscopy and Gas Chromatography (GC) with mass
96 spectrometry (MS). The capacity of T2H to form SOA by reaction with ozone was
97 investigated for the first time using a Scanning Mobility Particle Sizer (SMPS) device and
98 aerosol yields were evaluated.

99 2. MATERIALS AND METHODS

100 2.1. Reactors, conditions and reagents

101 Four experimental setups were used in the present study: A Laminar Flow Reactor (LFR)^[7,26]
102 and an Atmospheric Simulation Chamber (ASC)^[27,28] at IMT Lille Douai, a glass chamber^[29]
103 at Wuppertal University and a Rigid Atmospheric Simulation Chamber (RASC)^[22,30] at
104 GSMA/Reims University. While these reactors are briefly described in this section, the reader
105 is invited to refer to the cited literature for more details. A summary of the experimental

106 conditions and analytical techniques is provided in Table 1. The compounds used with stated
107 purities are reported in SI.

108 **2.1.1 LFR/IMT Lille Douai (France)**

109 The LFR was used to study the kinetics of T2H + O₃ in a dynamic flow reactor in the absence
110 of an OH scavenger. The reactor consists in a vertical Pyrex tube of 1 m length and 10 cm
111 inner diameter working with a total flow of 2.3 L min⁻¹. Accurate concentrations of T2H were
112 prepared in canisters through vaporization of small aldehyde aliquots and filled with air to a
113 pressure of approximately 3 bars. A small flow (typically 10 mL min⁻¹) from the canister was
114 diluted by purified air and then sent to the reactor injection head. GC coupled to a thermal
115 desorption system was used in online mode for the sampling and analysis of the organic
116 reactant. A double detection by flame ionization (FID) and mass spectrometry (MS) was
117 operated on the GC. The initial concentration of T2H was calculated from the FID signal
118 using the calibration curve determined in preliminary work. Ozone was produced by flowing
119 oxygen through an ozone generator (TEI 146) and was analyzed by a UV-absorption based
120 analyzer.

121 **2.1.2 ASC/IMT Lille Douai (France)**

122 The ASC was used to determine the rate constant with and without OH scavenger
123 (cyclohexane) and to investigate the SOA formation from the studied reaction. It consists of a
124 Teflon bag of about 300 L inside a wooden box, which ensures darkness during experiments.
125 Two ports installed on the reactor walls allow filling and emptying of the reactor and taking
126 gas samples for analyses. Ozone was produced by flowing purified air through a high-voltage
127 discharge generator (C-Lasky Ozone Generator). Ozone was measured using the same
128 analyzer as in LFR experiments. T2H and cyclohexane were quantified by FTIR using a 2 L
129 White cell with 10 m optical path. Mid-IR spectra were recorded every 4 min with a
130 resolution of 0.5 cm⁻¹ (100 spectra co-added). The initial concentration of T2H was calculated
131 from IR spectra using a calibration curve determined in preliminary work. The
132 characterization of particles in the reactor was carried out with an SMPS with a sampling flow
133 of 0.6 L min⁻¹ at a scan rate of 2.5 min (particle size distribution 10 – 408 nm).

134 **2.1.3 480-L glass-Wuppertal University (Germany)**

135 The 480-L glass chamber, characterized with a 3 m length and an inner diameter of 45 cm,
136 was used to study the reaction products without adding an OH scavenger. Yet, some

137 experiments were performed with dimethyl-ether as OH tracer. Different ports allow the
138 addition of both reagents and bath gases. Ozone was generated by a homemade device via
139 corona discharge in a flow of oxygen. To evacuate the chamber, a pumping system made of a
140 roots pump backed by a double stage rotary pump is used. In order to ensure the homogeneity
141 of the reaction mixture, a Teflon fan is mounted inside the reactor. The concentrations of
142 reactants and products were determined by IR spectroscopy using a FTIR spectrometer with a
143 multi-reflection mirror system operating at an optical path length of 50.4 m, mounted
144 internally in the chamber. Spectra were recorded every 5 min with a spectral resolution of 1
145 cm^{-1} (70 spectra co-added). The initial concentration of T2H was obtained using a calibration
146 method described previously^[31].

147 2.1.4 RASC - GSMA Reims (France)

148 The RASC was used to determine the reaction products in the presence of an OH radical
149 scavenger. It is a 63-L triple jacket Pyrex cell with an inner diameter of 20 cm and a total
150 length of 2 m. A set of spherical golden mirrors placed in the cell ensures multiple reflections
151 and allows us to get an optical path of 56 m. This chamber was coupled to an FTIR
152 spectrometer and to a GC/MS. Spectra were recorded every 3 min with a spectral resolution
153 of 2 cm^{-1} (100 spectra co-added). Ozone was produced according to the procedure given by
154 Griggs^[32]. Its concentration was monitored by UV absorption spectroscopy using a CCD
155 camera and then continuously driven into the simulation chamber. The concentrations of the
156 reagents and the products formed during the ozonolysis reaction were monitored by IR and by
157 Solid Phase Micro-Extraction (SPME)-GC/MS (see SI section B for more details) and were
158 corrected for the pressure increase (about 200 Torr per hour).

159 2.2. Kinetic measurements

160 All experiments in ASC and LFR were carried out under pseudo-first-order conditions where
161 the initial aldehyde concentration was in excess by a factor of 10 or more compared to that of
162 ozone (Table 1). With OH radicals being produced in the $\text{O}_3 + \text{T2H}$ reaction^[20] and OH
163 reacting fast with T2H ($k(\text{OH}+\text{T2H}) = 4.24 \times 10^{-11} \text{ cm}^3 \text{ molecule}^{-1} \text{ s}^{-1}$ ^[17-19]), some experiments
164 in the chamber were performed with cyclohexane as OH scavenger.

165 In the ASC reactor, a typical experiment was performed as follows: T2H was introduced into
166 the reactor and allowed to homogenize for around 30 min. Four samples were then taken to
167 determine its initial concentration. Where applicable, a sufficient quantity of cyclohexane was
168 added to trap about 94% of the formed hydroxyl radical (see SI section C) and the

169 T2H/cyclohexane mixture was allowed to homogenize for 1 hour. Subsequently, three
 170 samples were taken to quantify the initial concentration of both T2H and cyclohexane and to
 171 verify that there is no interference between the selected IR bands of the two compounds.
 172 Ozone was then introduced into the reactor and continuous O₃ measurements were performed
 173 over time.

174 Concerning experiments carried out in the LFR, ozone was introduced in a continuous flow
 175 through the injection head which was moved up and down to change the reaction time from
 176 30 s to about 3 min. The remaining ozone is measured for each position of the reactor's head.

177 Ozone wall losses ($k_{\text{wall loss}}$) in the ASC chamber and the LFR reactor were estimated in
 178 preliminary tests. The obtained $k_{\text{wall loss}}$ were of $3 \times 10^{-5} \text{ s}^{-1}$ and $1.55 \times 10^{-6} \text{ s}^{-1}$ in the ASC and
 179 LFR, respectively. T2H wall losses were also investigated both in the ASC and the LFR and
 180 were found to be negligible.

181 The consumption of ozone can be expressed as follows:

$$-\frac{d[O_3]}{dt} = k[T2H]_0[O_3] + k_{\text{wall loss}}[O_3] = k'[O_3] \quad (\text{Eq. 1})$$

182 where $k' = k[T2H]_0 + k_{\text{wall loss}}$. Since the aldehyde is in excess over O₃, the integration of Eq. 1
 183 gives:

$$\ln\left(\frac{[O_3]_0}{[O_3]}\right) = k't \quad (\text{Eq. 2})$$

184 where $[T2H]_0$ and $[O_3]_0$ are respectively the initial concentrations of T2H and ozone and $[O_3]$
 185 is the concentration of ozone at time t . Eq. 1 shows that the measured ozone decays are only
 186 dependent on T2H concentration and O₃ wall losses and will thus not be affected by the
 187 presence or absence of an OH scavenger^[23]. In the case of LFR, the reaction time is calculated
 188 using the expression computed by Duncianu et al.^[26] taking into account the slight parabolic
 189 form of the flow rate profile in the reactor^[26]. According to Eq. 2, the slope of the linear
 190 fitting of $\ln\left(\frac{[O_3]_0}{[O_3]}\right)$ versus time gives the pseudo-first-order rate constant k' . The ozonolysis
 191 rate constant k can be determined from the slope of the plot of k' as a function of $[T2H]_0$.

192 2.3. Product analysis

193 The experiments were performed in the 480-L glass reactor without OH scavenger and in the
 194 RASC chamber using cyclohexane as OH scavenger (see Table 1 for initial concentrations).

195 Product yields Y_{Prod} were obtained from the plot of the product mixing ratios [Prod] vs.
196 aldehyde consumption, $\Delta[T2H]$, according to Eq. 3.

$$Y_{Prod} (\%) = \frac{[Prod]}{\Delta[T2H]} \times 100 \quad (\text{Eq. 3})$$

197 **2.3.1. Product analysis in the 480-L glass reactor**

198 The products were identified and quantified by FTIR spectroscopy, where recorded spectra
199 were compared with references available in IR databases at the Wuppertal laboratory. The
200 quantification of butanal was done using tabulated IR absorption cross sections determined in
201 the same system. Glyoxal was quantified using absorption cross sections determined by
202 Volkamer et al.^[33]. T2H, butanal and glyoxal concentrations were retrieved using the
203 following IR absorption bands centered at 1150 and 2726 cm^{-1} , 1126 and 2712 cm^{-1} , and 2835
204 cm^{-1} , respectively, by iterative subtraction of calibrated reference spectra. Uncertainties on
205 Y_{Prod} were obtained by adding errors on $\Delta[T2H]$ (estimated at 14%) and errors on [Prod]
206 arising from uncertainties on both absorption cross sections (5%) and subtraction procedure
207 (10%). Overall uncertainties on Y_{Prod} calculated by error propagation were of the order of
208 20%.

209 **2.3.2. Product analysis in the RASC chamber**

210 Two techniques were used to identify and quantify the products in the RASC chamber: FTIR
211 spectroscopy and SPME-GC/MS. The derivatization conditions were taken from Reisen et
212 al.^[34] and are summarized in SI (section B). During each experiment, T2H and cyclohexane
213 were driven by an air flow into the simulation chamber. The ozonolysis reaction started
214 following the addition of ozone into the chamber through a continuous flow. The sampling
215 was carried out every 15 min and the analyses were performed by GC-MS. At the same time,
216 IR spectra were recorded every 3 min and T2H (1615-1674 cm^{-1}) and 2-hydroxybutanal
217 (1043-1077 cm^{-1}) bands were processed and integrated. The areas of the chromatographic
218 peaks or IR bands were related to the concentration of the product through calibration curves
219 previously prepared for the different compounds.

220 The formation yields of all stable primary and secondary products were determined by SPME-
221 GC/MS. IR spectra were only used to identify and quantify 2-hydroxy-butanal (IR reference
222 spectrum in Figure S1). The obtained yields correspond to the average of three experiments.
223 Overall uncertainties on the yields were calculated by error propagation considering both the

224 repeatability of the measurements and errors on spectra subtractions, peak integrations and
225 calibration procedures. The overall uncertainties on yields vary from 25-30%.

226 2.4. SOA formation

227 Particle formation was studied in ASC in the absence of OH scavenger. Preliminary tests were
228 performed to ensure that no particle formation occurs when either T2H or ozone was
229 introduced alone in the chamber. Continuous SMPS measurements started just after ozone
230 injection until a steady state of particle mass formation was reached.

231 The relatively high surface-to-volume (S/V) ratio of the reactor ($\sim 7 \text{ m}^{-1}$) inevitably led to
232 semi-volatile gas and particle losses on the walls^[35]. Aerosol wall losses were determined for
233 each experiment after maximum aerosol formation, resulting in first-order decay rates of 10-
234 20% h^{-1} . The aerosol mass concentrations measured in the present work were then corrected
235 for wall losses. SOA formation yields (Y_{SOA}) were calculated according to the following
236 expression:

$$Y_{\text{SOA}} (\%) = \frac{M_0}{\Delta[\text{T2H}]_f} \times 100 \quad (\text{Eq. 4})$$

237 where M_0 is the corrected maximum mass concentration of particles formed and $\Delta[\text{T2H}]_f$ is
238 the consumed mass concentration of T2H at the same time. Total aerosol mass concentrations
239 M_0 were calculated from the measured number size distributions assuming spherical particles
240 with a density of 1 g cm^{-3} . The experimental conditions including, initial concentrations and
241 analytical techniques are summarized in Table 1.

242 3. RESULTS AND DISCUSSION

243 3.1. Kinetics

244 The pseudo-first order rate constant k' was determined according to Eq. 2 from the plot of
245 $\ln([\text{O}_3]_0/[\text{O}_3])$ versus reaction time (Figures S2 (chamber) and S3 (flow reactor)). The data
246 were fitted with linear regression lines. Plots in Figure S2 and S3 display a good linearity with
247 high correlation coefficients ($R^2 > 0.90$). A linear regression of the k' data vs. $[\text{T2H}]_0$ (Figure
248 1) yields the second order rate constant. A value of $k(\text{T2H} + \text{O}_3) = (1.52 \pm 0.19) \times 10^{-18} \text{ cm}^3$
249 $\text{molecule}^{-1} \text{ s}^{-1}$ was obtained where the statistical uncertainty represents 2σ (fitting error). This
250 k -value comes from a fit on both ASC and LFR data.

251 Statistical errors on k' (2σ) resulting from the fitting procedure and reported on Figure 1 are
252 2-6% for ASC data and 9-26% for LFR data. $[T2H]_0$ is determined with an uncertainty of
253 about 10% arising from the calibration procedure. Systematic errors on $[T2H]_0$ that may
254 impact k values are probably negligible because of the high volatility of T2H leading to a
255 quantitative injection in the reactor. Propagating the errors results in a global uncertainty on k
256 of about 16%.

257 The obtained value is in good agreement with data obtained in simulation chambers (Table 2).
258 The rate constant was first determined by Atkinson et al.^[20] using the relative kinetic method.
259 They reported a value of $2 \times 10^{-18} \text{ cm}^3 \text{ molecule}^{-1} \text{ s}^{-1}$ with an uncertainty of 50%. Grosjean et
260 al.^[23] used pseudo-first order conditions with T2H in excess and obtained a value of
261 $(1.28 \pm 0.28) \times 10^{-18} \text{ cm}^3 \text{ molecule}^{-1} \text{ s}^{-1}$. More recently, Kalalian et al.^[22] obtained
262 $(1.37 \pm 0.03) \times 10^{-18} \text{ cm}^3 \text{ molecule}^{-1} \text{ s}^{-1}$ in absolute rate experiments. As can be seen, the present
263 value of $(1.52 \pm 0.19) \times 10^{-18} \text{ cm}^3 \text{ molecule}^{-1} \text{ s}^{-1}$ agrees very well with those of Grosjean et al.
264 and Kalalian et al. and is consistent with that of Atkinson et al. taking into account the
265 uncertainties. The present work represents the first determination of $k(T2H + O_3)$ in a flow
266 reactor. The present results also complement the study of Grosjean et al.^[23] which was carried
267 out using the absolute kinetics method and T2H in excess, yet with a much narrower range of
268 T2H concentrations than our study (Table 2). The very good agreement with Grosjean et al.
269 adds to the reliability of the results.

270 The $T2H + O_3$ reaction rate constant is significantly higher than that reported for acrolein (a
271 mono-substituted unsaturated compound, $3.5 \times 10^{-19} \text{ cm}^3 \text{ molecule}^{-1} \text{ s}^{-1}$)^[36] whereas it is in the
272 same order of magnitude as that of other longer (bi-substituted) unsaturated aldehydes:
273 crotonaldehyde $((1.58-1.74) \times 10^{-18} \text{ cm}^3 \text{ molecule}^{-1} \text{ s}^{-1})$ ^[37,38]; 2-pentenal $(1.6 \times 10^{-18} \text{ cm}^3$
274 $\text{molecule}^{-1} \text{ s}^{-1})$ ^[38], and a series of linear C_7 - C_9 unsaturated aldehydes: 2-heptenal, 2-octenal
275 and 2-nonenal $((2.05-2.47) \times 10^{-18} \text{ cm}^3 \text{ molecule}^{-1} \text{ s}^{-1})$ ^[39]. This suggests the role of the $C=C$
276 double bond substitution on the reactivity of alkenals towards O_3 , with a positive inductive
277 effect on the electronic density of the $C=C$ bond and an increase of the O_3 addition rate
278 constant from mono- to bi-substituted alkenals.

279 McGillen et al. proposed a structure-activity relationship for the ozonolysis kinetics of a
280 number of unsaturated compounds including aldehydes^[40]. They underlined the role of the
281 inductive effect on the reactivity of these species. For T2H, an ozone rate constant of 2.0×10^{-18}
282 $\text{cm}^3 \text{ molecule}^{-1} \text{ s}^{-1}$ can be calculated, which is in good agreement with experimental

283 findings. Comparing the rate constant for the ozonolysis of T2H to that of trans-2-hexene
284 ($155 \times 10^{-18} \text{ cm}^3 \text{ molecule}^{-1} \text{ s}^{-1}$)^[41] shows a 100 times higher rate constant for the homologous
285 alkene compared to the studied aldehyde. A similar trend is observed for
286 crotonaldehyde/trans-2-butene^[41,42] and 2-pentenal/trans-2-pentene^[41]. This shows the strong
287 deactivating effect of the carbonyl group on the reactivity of the C=C double bond towards
288 ozone through the conjugation of the two π systems (C=O and C=C).

289

290 3.2. Product formation

291 3.2.1. Product formation investigated in 480-L glass reactor

292 Seven experiments were performed in the 480-L glass reactor, out of which three included
293 dimethyl ether (DME) used as OH radical tracer. Based on the DME pseudo-first order
294 consumption, an upper limit of $10^6 \text{ molecules cm}^{-3}$ was estimated for the concentration of OH
295 radicals in this reaction system. Butanal and glyoxal were identified as the major primary
296 products by FTIR. The fine spectral features of glyoxal can be clearly observed in the 2800-
297 2850 cm^{-1} region while the presence of butanal is evidenced near 2700 cm^{-1} (Figure 2). After
298 subtracting T2H and O_3 as well as glyoxal and butanal, the residual spectra show features that
299 indicate the presence of products containing carbonyl and possibly OH moieties.

300 Concentration-time profiles of T2H, butanal and glyoxal are presented in Figure S4 together
301 with the carbon balance calculated as molar yield. Yield plots of the concentrations of the
302 primary products as a function of consumed T2H are shown in Figure 3, for all performed
303 experiments. For butanal and glyoxal, molar yields of $33 \pm 7\%$ and $48 \pm 10\%$, respectively, were
304 obtained, where the errors (2σ) represent estimated total uncertainties of $\sim 20\%$ (see section
305 2.3.1). These yields were not corrected for potential OH losses. The OH concentration
306 evaluated upon tracer data ($10^6 \text{ molecules cm}^{-3}$) is rather small to compete significantly with
307 the T2H + O_3 reaction considering the ozone concentrations used, namely $(4-8) \times 10^{14}$
308 molecules cm^{-3} .

309 The formation of propanal could be observed in all experiments (see Figure S5) but due to
310 overlapping of absorption features it cannot be quantified accurately. An upper limit of 8%
311 (molar yield) can be estimated using the absorption band centered at 2992 cm^{-1} . Similarly, it is
312 not possible to quantify acetaldehyde in the residual spectra although there are features
313 indicating its formation (Figure S5). From the residual spectra and using the absorptions

314 centered at 1352 and 2706 cm^{-1} , respectively, an upper limit of 10% can be calculated for the
315 molar yield of acetaldehyde.

316 Although a significant increase was observed for the intensity of the specific absorptions
317 attributed to CO and CO₂, their quantification is not possible under the present experimental
318 setup due to interferences of these compounds present in the dry air used to flush the transfer
319 optics housing between the chamber and FTIR spectrometer. Formaldehyde was not observed
320 in the IR spectra. Considering the detection limit of 200 ppb in our system, an upper limit of
321 4% can be deduced for the molar yield of formaldehyde, if any.

322 **3.2.2. Product formation investigated in RASC chamber**

323 Five carbonyl compounds: glyoxal, butanal, propanal, acetaldehyde and 2-hydroxybutanal
324 were positively identified in the gas-phase reaction of T2H with O₃, in the presence of
325 cyclohexane as OH scavenger. CO was not observed while CO₂ analysis was precluded due to
326 the lack of a specific instrument. 2-Hydroxybutanal was detected both in the residual IR
327 spectra (after subtraction of the known features, a significant absorption band persisted
328 between 1043 and 1077 cm^{-1} which can be assigned to 2-hydroxybutanal) and by GC/MS
329 through the corresponding oxime. The temporal evolution of the molar fractions of T2H and
330 of the products formed during the ozonolysis reaction as well as the carbon balance are
331 presented in Figure S6. Product concentrations are relatively stable after 60 min. The carbon
332 balance decreases with the T2H + O₃ reaction progress, indicating the formation of other
333 undetected products. Formation yields of primary and secondary products were determined by
334 plotting product concentrations as a function of the consumed T2H (Figure 4). The 2-
335 hydroxybutanal yields obtained by IR and GC/MS techniques were in good agreement with a
336 difference lower than 20%. The products identified and quantified by FTIR (480-L chamber,
337 RASC) and GC/MS (RASC) are summarized in Table 3.

338 **3.2.3. Comparison with literature data**

339 Glyoxal and butanal have been identified as main products in both the 480-L reactor and
340 RASC. The product yields obtained in both set-ups are in good agreement (48±10% and
341 33±7% in the 480-L reactor, Figure 3, 59±15% and 36±9% in RASC, Figure 4) within the
342 uncertainties and thus seem not to be influenced by the formation of OH during the ozonolysis
343 reaction.

344 In the 480-L chamber, the concentration of OH radicals was estimated based on the tracer
345 (DME) consumption to vary from 10⁵ to 10⁶ molecules cm^{-3} . By using the method described

346 by Klotz et al.^[43] to correct for the OH reaction, this accounts for up to 10% of the overall
347 consumption of trans-2-hexenal. Further, this finding suggests a much lower OH yield from
348 the T2H + O₃ reaction as previously reported^[20]. A former study^[44] on the ozonolysis of trans-
349 2-alkenals estimates an OH production of up to 15% which is supported by our results using
350 DME (Figure S7). This indicates that the errors in the experimentally determined yields for
351 butanal and glyoxal are higher than the effect of the presence of OH in the reaction system.
352 Nevertheless, the yields are slightly below the values obtained when using an OH scavenger
353 (RASC).

354 The results are summarized in Table 3 together with literature data^[23]. The glyoxal yields
355 determined here are in good agreement with the previous study carried out by Grosjean et al.,
356 who normalized the carbonyl concentration to the concentration of reacted ozone. In both
357 chambers in this study, the butanal yield is somewhat lower than previously reported. Unlike
358 Grosjean et al., whose results suggest that both main products are formed in equal portions,
359 the present study indicates a slight preference for the pathway yielding the bicarbonyl
360 compound, namely glyoxal. The ozonolysis of asymmetric alkyl-substituted alkenes is known
361 to favor the formation of the most substituted bi-radical due to hyperconjugation^[23,45].
362 Further, studies carried out on the ozonolysis of oxygenated alkenes indicate that the
363 decomposition of the primary ozonide displays a preference for the pathway yielding an
364 oxygenated carbonyl^[46-48]. Hence, the formation of the alkyl-substituted bi-radical and the
365 formation of glyoxal could be favored. However, the limited number of reported data for the
366 ozonolysis of trans-2-alkenals (C₃-C₉, Table S1) does not indicate a clear trend to support this
367 observation.

368 When comparing with the studies performed by Grosjean and co-workers, one notes that they
369 worked at a relative humidity of 55%^[23] whereas the present study was done under dry
370 conditions (RH ≤ 1%). At least for glyoxal, it was determined that aerosols represent a
371 significant sink due to reactive uptake on surface,^[4,49,50] especially at high RH^[51,52]. For
372 butanal and trans-2-hexenal, presently no such information is available, therefore further
373 considerations would be highly speculative. The fate of the stabilized Criegee Intermediates
374 (CI) that are expected to come from O₃ + T2H is also highly dependent on the amount of
375 water available.^[3,7] Since butanal and glyoxal do not come from CI, their yields are not
376 expected to be impacted by RH.

377 Acetaldehyde, propanal and 2-hydroxybutanal were undoubtedly quantified only in RASC.
378 The yield of acetaldehyde is in excellent agreement with the previous determination by

379 Grosjean et al.^[23]. There is evidence of formation of propanal and acetaldehyde in the 480-L
380 chamber (Figure S5), however the quantification limit of the system and the superposition of
381 the spectra allows only the estimation of upper limits for their yields. The presence of
382 butanoic acid in the spectra obtained from the 480-L chamber cannot be ruled out as its
383 spectral features can be “hidden” beneath the residual unidentified absorptions (Figure S8).

384 The residual spectra of the experiments with OH scavenger (Figure 2, panel E), after
385 subtracting T2H, ozone and the main products, contain additional absorption features which
386 suggest formation of unidentified carbonyl containing compounds and which differ from the
387 absorption of 2-hydroxybutanal recorded in RASC. However, the characteristic absorption
388 system between 3000 cm^{-1} and 2700 cm^{-1} looks similar to the residual spectra reported by
389 Colman et al.^[44]. They studied the ozonolysis of longer trans-2-alkenals and tentatively
390 assigned their residuals to the corresponding 2-oxoaldehydes. Grosjean et al.^[23] identified 2-
391 oxobutanal in the ozonolysis of trans-2-hexenal with a yield of $7.4\pm 0.6\%$. However, they
392 argued that, due to the use of dinitrophenylhydrazine derivatization, followed by offline high
393 performance liquid chromatography to identify and quantify products, they were not able to
394 distinguish between the 2-oxo and the 2-hydroxyaldehyde. The results obtained presently in
395 RASC indicate that rather 2-hydroxybutanal is formed than 2-oxobutanal.

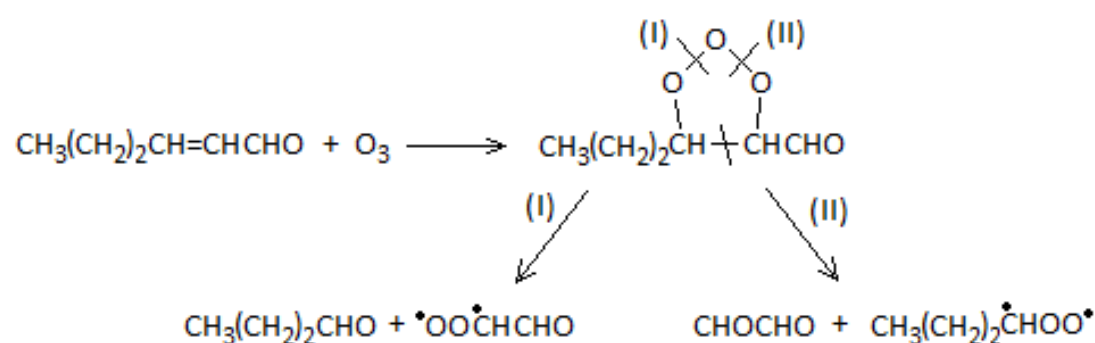
396 The organic gas-phase carbon balance calculated in RASC is lower than 100% (down to 60%
397 at the end), and even lower in the 480-L chamber. One reason is the impossibility to
398 determine all products formed in such a complex system, as stated above. The ozonolysis
399 reactions are generally known to deliver poor overall yields as the identification and
400 quantification of all products often fails^[53]. On the other hand, the formation of aerosol
401 particles observed here strongly suggests that the adsorption on particles and/or heterogeneous
402 chemistry is possibly responsible for incomplete carbon numbers. At this time, without
403 knowledge on the particle composition, it is not possible to make a quantitative estimation of
404 the contribution of aerosols to the carbon balance in the ozonolysis of trans-2-hexenal.

405 **3.2.4. Mechanism**

406 The products identified within this study support a classical approach, namely the
407 electrophilic addition of O_3 to the double bond followed by the decomposition of the ozonide
408 into a primary carbonyl and a Criegee biradical (CI)^[3]. A reaction mechanism for T2H
409 ozonolysis is proposed in Figure 5 based on the product analysis from the RASC and 480-L
410 chambers.

411 The first step in the ozonolysis of trans-2-hexenal will produce an asymmetrical ozonide. As
 412 displayed in Scheme 1, there are two possibilities for it to dissociate.

413



414

415 **Scheme 1.** Ozone addition to T2H followed by decomposition of the ozonide according to
 416 two channels: (I) forming butanal and (II) forming glyoxal as primary carbonyls.

417

418 Channel (I) leads to the formation of butanal identified and quantified in this work as a major
 419 product. The $\cdot\text{OO}\cdot\text{CHCHO}$ biradical resulting from channel (I) could evolve into two
 420 pathways (Figure 5):

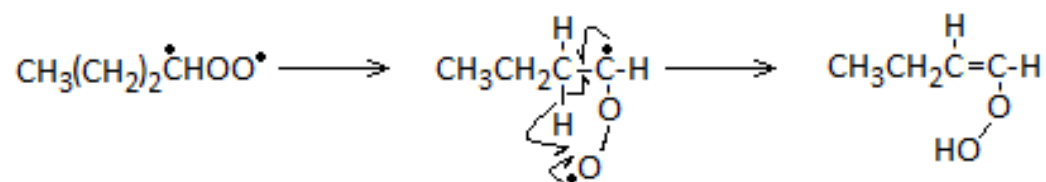
- 421 a. Formation of formaldehyde and CO_2 : Formaldehyde was not observed in the FTIR
 422 spectra, neither in the 480-L nor in the RASC chamber. Although an increase in
 423 the intensity of the characteristic CO_2 absorptions bands ($2289\text{-}2388\text{ cm}^{-1}$) was
 424 observed, its quantification was not possible under the given experimental
 425 conditions. According to the limit of detection for formaldehyde in the 480-L
 426 chamber, the branching ratio for this channel, if occurring, is below 0.04.
- 427 b. OH and $\text{CHOCO}\cdot$ formation. The $\text{CHOCO}\cdot$ radical could evolve into CO_2 and
 428 $\text{CHO}\cdot$, the latter reacting with O_2 to form HO_2 and CO. The formation of OH
 429 radicals was observed in the 480-L chamber in absence of scavenger, using DME
 430 as a tracer. Carbon monoxide formation was unambiguously observed in the IR
 431 spectra recorded in the 480-L chamber but no quantification was possible for
 432 reasons mentioned earlier. We envision a systematic determination of both CO and
 433 OH yields as the object of a future study.

434

435 Channel (II) leads to the formation of glyoxal, another major product identified and quantified
 436 in our study. The vibrationally excited CI from channel (II) could either be stabilized by

437 collision or undergo fast unimolecular decomposition i) via 1,5-H shift and hydroperoxide
 438 formation (Scheme 2) or ii) to form OH and an alkoxy radical that leads to propanal (Figure
 439 5).

440



441

442 **Scheme 2.** The hydroperoxide channel – the fate of the excited CI resulting from channel (II).

443

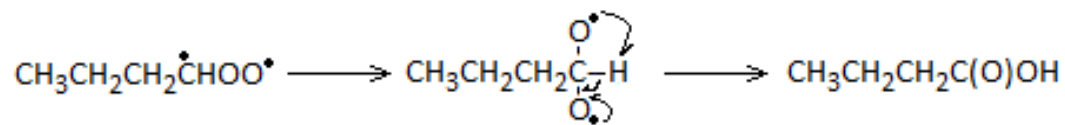
444 The hot hydroperoxide resulting from channel (II) as presented in Scheme 2 can evolve into
 445 four different pathways (Figure 5)^[54]:

- 446 a'. Rearrangement into and stabilization of a β -hydroxycarbonyl: 2-hydroxybutanal
 447 was observed in RASC with a formation yield of $18 \pm 6\%$;
- 448 b'. Formation of H_2 and 2-oxobutanal: the formation of 2-oxobutanal in the present
 449 study cannot be ruled out;
- 450 c'. Decomposition into $CHO^\bullet + \alpha$ -hydroxyalkyl, the latter yielding propanal, observed
 451 in the present work in the experiments with an OH scavenger and quantified with a
 452 formation yield of $19 \pm 5\%$ in RASC; CHO^\bullet will yield $HO_2 + CO$; as mentioned
 453 above, CO formation was observed by IR but not quantified;
- 454 d'. Release of an OH radical and formation of $CH_3CH_2\dot{C}HCHO$. In the presence of
 455 O_2 , this radical will form the oxy radical $CH_3CH_2CHO^\bullet CHO$. The oxy radical
 456 further chemistry may evolve toward production of acetaldehyde, glyoxal, propanal
 457 and 2-oxobutanal. Acetaldehyde was identified and quantified in our study with a
 458 formation yield of around 10%.

459 In the proposed mechanistic scheme, propanal, acetaldehyde and 2-hydroxybutanal are solely
 460 formed from CI (II) through the hydroperoxide channel (pathways a', c' and d'). The yield for
 461 glyoxal formed via route d'₁ should be equal to the acetaldehyde yield (see Figure 5). It is
 462 worth noting that for RASC (taking into account the uncertainties) the sum of propanal,
 463 acetaldehyde and 2-hydroxybutanal yields (47%) differs by roughly 10% from the glyoxal
 464 yield (59%). This is consistent with the proposed mechanism.

465 In addition to the evolution routes mentioned above, the stabilized biradical
 466 $\text{CH}_3(\text{CH}_2)_2\text{C}^{\bullet}\text{HOO}^{\bullet}$ can isomerize into a dioxy biradical and form butanoic acid (Scheme
 467 3)^[3,55].

468



469

470 **Scheme 3.** Formation of butanoic acid from the stabilized CI $\text{CH}_3(\text{CH}_2)_2\text{C}^{\bullet}\text{HOO}^{\bullet}$ arising from
 471 channel (II).

472

473 No certain identification of butanoic acid is possible due to IR absorption band overlapping in
 474 the residual spectra (see Figure S8). Thus, the formation of an organic acid cannot be
 475 excluded.

476 3.3. SOA formation

477 Aerosol formation was investigated in the 300-L Teflon chamber. SOA growth is presented
 478 below in terms of total produced mass concentrations and aerosol yields.

479 3.3.1 Particle mass concentrations

480 Figure 6 shows particle formation, in terms of corrected mass concentration M_0 , as a function
 481 of time in the ASC chamber. According to Figure 6, particle formation in ASC is very fast
 482 and occurred as soon as ozone is injected. SOA mass concentrations reach a plateau after
 483 roughly 50 min reaction time after which M_0 stabilizes. It is important to stress that the
 484 decreasing carbon balance observed with reaction time could be partly explained by the
 485 increasing organic matter in the condensed phase.

486 3.3.2 Yield plots

487 From SOA mass concentrations at the maximum of the plateau together with the
 488 corresponding T2H consumption, aerosol yields can be determined according to Eq. 4. Figure
 489 7 displays the aerosol yield as a function of aerosol mass concentration for the experiments
 490 carried out in ASC. The oxidation of 1.6 to 10.2 ppm of aldehyde by increasing amount of
 491 ozone led to SOA yields of 3.2% to 13.4% for T2H corresponding to SOA mass

492 concentrations up to $418 \mu\text{g m}^{-3}$. The Y_{SOA} vs. M_0 data were fitted using the one-product
 493 model from Odum et al.^[56] that translates into the following equation:

$$Y_{\text{SOA}} = M_0 \left(\frac{\alpha K_{\text{om}}}{1 + M_0 K_{\text{om}}} \right) \quad (\text{Eq. 5})$$

494 where α is the mass-based gas-phase stoichiometric coefficient of a model product and K_{om}
 495 represents its gas-particle partitioning equilibrium constant. α represents the total amount of
 496 semi-volatile products present in the gas- and aerosol- phases. A least-square regression on
 497 the data yields gives the following parameters: $\alpha = 0.22 \pm 0.08$ and $K_{\text{om}} = (3.2 \pm 2.4) \times 10^{-3} \text{ m}^3$
 498 μg^{-1} . Uncertainties represent two standard deviations (2σ). Comparing α with Y where Y
 499 corresponds to the semi-volatile products in the particle phase indicates that only a fraction of
 500 the semi-volatile products go into the condensed phase.

501 3.3.3 Atmospheric impact

502 The present study shows for the first time that ozonolysis reactions for T2H can be a
 503 significant source of particles. As shown in Figure 7, an increase in the aerosol mass
 504 concentration leads to higher yields, consistent with increased surface area onto which
 505 condensation/partitioning of condensable reaction products can occur. In indoor environments
 506 where particle concentrations are often much higher than outdoor, sometimes by one order of
 507 magnitude^[57-59], up to 10% of the reacted T2H can go into the particulate phase, provided
 508 sufficient O_3 are present indoors. Further investigations in larger reactors are clearly needed to
 509 thoroughly quantify the potential of T2H and other alkenals to form SOA through ozonolysis.
 510 In the atmosphere where the atmospheric fate of T2H is mainly governed by its reaction with
 511 OH and NO_3 ,^[24] the impact of SOA formation from T2H ozonolysis is limited. The situation
 512 may be reversed indoors where OH and NO_3 radical concentrations are generally much lower
 513 than outdoors.^[60] Under these conditions, indoor sources of ozone – outdoor air as well as
 514 photocopiers and air purifiers – could make O_3 a significant oxidant indoors,^[60] thus
 515 potentially enhancing the contribution of T2H to SOA indoors. In some specific indoor cases,
 516 however, like high HONO levels or high- O_3 and low- NO concentrations, OH and NO_3 can
 517 reach high concentrations making T2H oxidation by OH and/or NO_3 significant indoors.^[60]

518 4. CONCLUSION

519 In this work, the kinetics of the reaction of T2H with ozone has been investigated for the first
 520 time using a flow reactor and the absolute method. Additional experiments using a static

521 atmospheric simulation chamber were performed. Both experimental set ups yield consistent
522 results and show very good agreement with the literature data.

523 The mechanistic studies carried out in the present work showed that the ozonolysis of T2H
524 leads to the formation of carbonyl compounds as primary products, namely glyoxal and
525 butanal, as well as acetaldehyde, propanal and 2-hydroxybutanal. In the presence of an OH
526 scavenger, molar yields of $59\pm 15\%$ and $36\pm 9\%$ were obtained for glyoxal and butanal,
527 respectively, in satisfactory agreement with the only reported study up to date^[23]. In the
528 absence of an OH scavenger, the yields of glyoxal and butanal did not differ significantly,
529 within the error limits, which suggests that secondary OH processes are of minor importance.
530 A detailed chemical reaction mechanism is proposed upon the identified reaction products.
531 The total yields of primary carbonyl products range between 81% and 95%. A slight
532 preference is directed towards the formation of the bi-radical not containing the aldehyde
533 function. These results on the C₆ alkenal complete the missing puzzle data of previous studies
534 of C₃-C₉ trans-2-alkenals.

535 Finally, the present study constitutes the first investigation of aerosol formation from the
536 ozonolysis of a trans-2-alkenal species, to the best of our knowledge. T2H ozonolysis is
537 shown to only slightly contribute to particle loadings in the atmosphere. Further work is
538 clearly needed to improve our understanding of SOA contribution from oxygenated
539 unsaturated compounds, which are ubiquitous species emitted by vegetation. Very recently,
540 Liu et al.^[61] suggested that alkenals contributed up to 34% of the SOA observed from the
541 photo-oxidation of vegetable oil emissions. Experimental work on reaction products and SOA
542 formation from T2H + OH is under progress, aiming at unravelling the role of this reaction in
543 the atmospheric chemistry of T2H.

544 **Acknowledgments**

545 IMT Lille Douai acknowledges funding by the French ANR agency under contract No. ANR-
546 11-LabX-0005-01 CaPPA (Chemical and Physical Properties of the Atmosphere), the Région
547 Hauts-de-France, the Ministère de l'Enseignement Supérieur et de la Recherche (CPER
548 Climibio) and the European Fund for Regional Economic Development. Part of this work has
549 received funding from the European Union's Horizon 2020 research and innovation program
550 through the EUROCHAMP-2020 Infrastructure Activity under grant agreement No 730997.
551 A. Grira is grateful for a PhD grant from Brittany Region and IMT Lille Douai. Authors from
552 French laboratories acknowledge the INSU-LEFE-CHAT program for funding this research.

553

554 **Bibliography**

- 555 [1] A. Guenther, C. N. Hewitt, D. Erickson, R. Fall, C. Geron, T. Graedel, P. Harley, L. Klinger, M.
556 Lerdau, W. A. McKay, T. Pierce, B. Scholes, R. Steinbrecher, R. Tallamraju, J. Taylor, P.
557 Zimmerman, *J. Geophys. Res. Atmospheres* **1995**, *100*, 8873–8892.
- 558 [2] R. Atkinson, J. Arey, *Atmos. Environ.* **2003**, *37*, S197–S219.
- 559 [3] D. Johnson, G. Marston, *Chem. Soc. Rev.* **2008**, *37*, 699–716.
- 560 [4] M. Hallquist, J. Wenger, U. Baltensperger, Y. Rudich, D. Simpson, M. Claeys, J. Dommen, N. M.
561 Donahue, C. George, A. H. Goldstein, J. F. Hamilton, H. Herrmann, T. Hoffmann, Y. Iinuma, M.
562 Jang, M. E. Jenkin, J. L. Jimenez, A. Kiendler-Scharr, W. Maenhaut, G. McFiggans, T. F. Mentel, A.
563 Monod, A. S. H. Prévot, J. H. Seinfeld, J. D. Surratt, R. Szmigielski, J. Wildt, *Atmospheric Chem.*
564 *Phys.* **2009**, *9*, 5155–5236.
- 565 [5] T. F. Stocker, D. Qin, G. K. Plattner, M. Tignor, S. K. Allen, J. Boschung, A. Nauels, Y. Xia, V. Bex,
566 P. M. Midgley, *IPCC, 2013: Climate Change 2013: The Physical Science Basis.*, Cambridge
567 University Press, **2013**.
- 568 [6] J. A. Thornton, J. E. Shilling, M. Shrivastava, E. L. D'Ambro, M. A. Zawadowicz, J. Liu, *ACS Earth*
569 *Space Chem.* **2020**, *4*, 1161–1181.
- 570 [7] W. Ahmad, C. Coeur, A. Cuisset, P. Coddeville, A. Tomas, *J. Aerosol Sci.* **2017**, *110*, 70–83.
- 571 [8] J. Laothawornkitkul, J. Taylor, N. D. Paul, C. N. Hewitt, *New Phytol.* **2009**, *183*, 27–51.
- 572 [9] J. Penuelas, M. Staudt, *Trends Plant Sci.* **2010**, *15*, 133–144.
- 573 [10] M. Toome, P. Randjäär, L. Copolovici, Ü. Niinemets, K. Heinsoo, A. Luik, S. M. Noe, *Planta* **2010**,
574 *232*, 235–243.
- 575 [11] E. Kleist, T. F. Mentel, S. Andres, A. Bohne, A. Folkers, A. Kiendler-Scharr, Y. Rudich, M. Springer,
576 R. Tillmann, J. Wildt, *Biogeosciences* **2012**, *9*, 5111–5123.
- 577 [12] A. Grira, C. Amarandei, M. N. Romanias, G. El Dib, A. Canosa, C. Arsene, I. G. Bejan, R. I. Olariu,
578 P. Coddeville, A. Tomas, *Atmosphere* **2020**, *11*, 256.
- 579 [13] X. Wang, J. Sun, L. Bao, Q. Mei, B. Wei, Z. An, J. Xie, M. He, *J. Phys. Chem. A* **2019**, *123*, 2745–
580 2755.
- 581 [14] L. Nondek, D. Rodler, J. W. Birks, *Environ. Sci. Technol.* **1992**, *26*, 1174–1178.
- 582 [15] J. Ehrlich, T. M. Cahill, *Atmos. Environ.* **2018**, *191*, 414–419.
- 583 [16] C. Warneke, S. L. Luxembourg, J. A. de Gouw, H. J. I. Rinne, A. B. Guenther, R. Fall, *J. Geophys.*
584 *Res. Atmospheres* **2002**, *107*, ACH 6-1-ACH 6-10.
- 585 [17] T. Gao, J. M. Andino, C. C. Rivera, M. F. Márquez, *Int. J. Chem. Kinet.* **2009**, *41*, 483–489.
- 586 [18] E. Jimenez, B. Lanza, E. Martinez, J. Albaladejo, *Atmospheric Chem. Phys.* **2007**, *7*, 1565–1574.
- 587 [19] M. E. Davis, M. K. Gilles, A. R. Ravishankara, J. B. Burkholder, *Phys. Chem. Chem. Phys.* **2007**, *9*,
588 2240–2248.
- 589 [20] R. Atkinson, J. Arey, S. M. Aschmann, S. B. Corchnoy, Y. Shu, *Int. J. Chem. Kinet.* **1995**, *27*, 941–
590 955.
- 591 [21] D. Rodriguez, A. Rodriguez, A. Notario, A. Aranda, Y. Diaz-de-Mera, E. Martinez, *Atmospheric*
592 *Chem. Phys.* **2005**, *5*, 3433–3440.
- 593 [22] C. Kalalian, E. Roth, A. Chakir, *Int. J. Chem. Kinet.* **2017**, *50*, 47–56.
- 594 [23] E. Grosjean, D. Grosjean, J. H. Seinfeld, *Int. J. Chem. Kinet.* **1996**, *28*, 373–382.
- 595 [24] C. Kalalian, B. Samir, E. Roth, A. Chakir, *Chem. Phys. Lett.* **2019**, *718*, 22–26.
- 596 [25] M. P. O'Connor, J. C. Wenger, A. Mellouki, K. Wirtz, A. Muñoz, *Phys. Chem. Chem. Phys.* **2006**, *8*,
597 5236–5246.
- 598 [26] M. Duncianu, R. I. Olariu, N. Visez, V. Riffault, A. Tomas, P. Coddeville, *J. Phys. Chem. A* **2012**,
599 *116*, 6169–6179.
- 600 [27] E. Turpin, A. Tomas, C. Fittschen, P. Devolder, J.-C. Galloo, *Environ. Sci. Technol.* **2006**, *40*, 5956–
601 5961.

- 602 [28] R. L. Caravan, M. A. H. Khan, J. Zádor, L. Sheps, I. O. Antonov, B. Rotavera, K. Ramasesha, K. Au,
603 M.-W. Chen, D. Rösch, *Nat. Commun.* **2018**, *9*, 1–9.
- 604 [29] I. Barnes, K. H. Becker, T. Zhu, *J. Atmospheric Chem.* **1993**, *17*, 353–373.
- 605 [30] L. Messaadia, G. El Dib, M. Lendar, M. Cazaunau, E. Roth, A. Ferhati, A. Mellouki, A. Chakir,
606 *Atmos. Environ.* **2013**, *77*, 951–958.
- 607 [31] T. Etzkorn, B. Klotz, S. Sorensen, I. V. Patroescu, I. Barnes, K. H. Becker, U. Platt, *Atmos. Environ.*
608 **1999**, *33*, 525–540.
- 609 [32] M. Griggs, *J. Chem. Phys.* **1968**, *49*, 857–859.
- 610 [33] R. Volkamer, P. Spietz, J. Burrows, U. Platt, *J. Photochem. Photobiol. Chem.* **2005**, *172*, 35–46.
- 611 [34] F. Reisen, S. M. Aschmann, R. Atkinson, J. Arey, *Environ. Sci. Technol.* **2003**, *37*, 4664–4671.
- 612 [35] P. Ye, X. Ding, J. Hakala, V. Hofbauer, E. S. Robinson, N. M. Donahue, *Aerosol Sci. Technol.* **2016**,
613 *50*, 822–834.
- 614 [36] I. Al Mulla, L. Viera, R. Morris, H. Sidebottom, J. Treacy, A. Mellouki, *ChemPhysChem* **2010**, *11*,
615 4069–4078.
- 616 [37] E. Grosjean, D. Grosjean, *Int. J. Chem. Kinet.* **1998**, *30*, 21–29.
- 617 [38] K. Sato, B. Klotz, T. Taketsugu, T. Takayanagi, *Phys. Chem. Chem. Phys.* **2004**, *6*, 3969–3976.
- 618 [39] E. G. Colman, M. B. Blanco, I. Barnes, M. A. Teruel, *R. Soc. Chem. Adv.* **2015**, *5*, 30500–30506.
- 619 [40] M. R. McGillen, A. T. Archibald, T. Carey, K. E. Leather, D. E. Shallcross, J. C. Wenger, C. J.
620 Percival, *Phys. Chem. Chem. Phys. PCCP* **2011**, *13*, 2842–2849.
- 621 [41] E. V. Avzianova, P. A. Ariya, *Int. J. Chem. Kinet.* **2002**, *34*, 678–684.
- 622 [42] R. Wegener, T. Brauers, R. Koppmann, S. R. Bares, F. Rohrer, R. Tillmann, A. Wahner, A. Hansel,
623 A. Wisthaler, *J. Geophys. Res. Atmospheres* **2007**, *112*, DOI 10.1029/2006JD007531.
- 624 [43] B. Klotz, I. Barnes, T. Imamura, *Phys. Chem. Chem. Phys.* **2004**, *6*, 1725–1734.
- 625 [44] E. Gaona Colman, M. B. Blanco, I. Barnes, P. Wiesen, M. A. Teruel, *J. Phys. Chem. A* **2017**, *121*,
626 5147–5155.
- 627 [45] E. C. Tuazon, S. M. Aschmann, J. Arey, R. Atkinson, *Environ. Sci. Technol.* **1997**, *31*, 3004–3009.
- 628 [46] E. Grosjean, E. L. Williams II, D. Grosjean, *Sci. Total Environ.* **1994**, *153*, 195–202.
- 629 [47] E. Grosjean, D. Grosjean, *J. Atmospheric Chem.* **1997**, *27*, 271–289.
- 630 [48] R. Uchida, K. Sato, T. Imamura, *Chem. Lett.* **2015**, *44*, 457–458.
- 631 [49] H. Shen, Z. Chen, H. Li, X. Qian, X. Qin, W. Shi, *Environ. Sci. Technol.* **2018**, *52*, 10997–11006.
- 632 [50] C. Knöte, A. Hodzic, J. L. Jimenez, R. Volkamer, J. J. Orlando, S. Baidar, J. Brioude, J. Fast, D. R.
633 Gentner, A. H. Goldstein, P. L. Hayes, W. B. Knighton, H. Oetjen, A. Setyan, H. Stark, R. Thalman,
634 G. Tyndall, R. Washenfelder, E. Waxman, Q. Zhang, *Atmospheric Chem. Phys.* **2014**, *14*, 6213–
635 6239.
- 636 [51] A. L. Corrigan, S. W. Hanley, D. O. De Haan, *Environ. Sci. Technol.* **2008**, *42*, 4428–4433.
- 637 [52] J. Liggio, S.-M. Li, R. McLaren, *J. Geophys. Res.* **2005**, *110*.
- 638 [53] A. Lee, A. H. Goldstein, M. D. Keywood, S. Gao, V. Varutbangkul, R. Bahreini, N. L. Ng, R. C.
639 Flagan, J. H. Seinfeld, *J. Geophys. Res.* **2006**, *111*, D07302.
- 640 [54] E. Grosjean, J. Bittencourt de Andrade, D. Grosjean, *Environ. Sci. Technol.* **1996**, *30*, 975–983.
- 641 [55] O. Horie, G. K. Moortgat, *Acc. Chem. Res.* **1998**, *31*, 387–396.
- 642 [56] J. R. Odum, T. Hoffmann, F. Bowman, D. Collins, R. C. Flagan, J. H. Seinfeld, *Environ. Sci. Technol.*
643 **1996**, *30*, 2580–2585.
- 644 [57] R.-J. Huang, Y. Zhang, C. Bozzetti, K.-F. Ho, J.-J. Cao, Y. Han, K. R. Daellenbach, J. G. Slowik, S. M.
645 Platt, F. Canonaco, *Nature* **2014**, *514*, 218–222.
- 646 [58] M. Corso, “Impact à court terme des particules en suspension (PM10) sur la mortalité dans 17
647 villes françaises, 2007-2010,” can be found under /determinants-de-sante/pollution-et-
648 sante/air/impact-a-court-terme-des-particules-en-suspension-pm10-sur-la-mortalite-dans-17-
649 villes-francaises-2007-2010, **2015**.
- 650 [59] L. Morawska, C. He, G. Johnson, H. Guo, E. Uhde, G. Ayoko, *Environ. Sci. Technol.* **2009**, *43*,
651 9103–9109.
- 652 [60] C. J. Young, S. Zhou, J. A. Siegel, T. F. Kahan, *Environ. Sci. Process. Impacts* **2019**, *21*, 1229–1239.
- 653 [61] T. Liu, Z. Wang, D. D. Huang, X. Wang, C. K. Chan, *Environ. Sci. Technol. Lett.* **2018**, *5*, 32–37.

Journal Pre-proof

Table 1. Summary of experimental conditions and analytical techniques used in the present work. All experiments were performed at room temperature (298 K) and atmospheric pressure of air (1 atm) except for RASC where the initial pressure was about 400 Torr.

Kinetic studies ^a					
Reactor-Laboratory	Reactor volume (L)	[O ₃] ₀ (ppm)	[T2H] ₀ (ppm)	OH Scavenger	Analytical techniques
LFR-IMT Lille Douai	10	0.555	6.5-25	Not used	- Ozone analyzer (Model 42M, Environnement SA) - GC-FID/MS (Agilent 6890-5973N)
ASC-IMT Lille Douai	300	0.113	≈4	Cyclohexane ^b	- Ozone analyzer (Model 42M, Environnement SA) - FTIR spectrometer (Thermo Nicolet 6700 with DTGS detector)
Product and SOA studies					
RASC-GSMA	63	< 1 ^d	20-25	Cyclohexane ^b	- FTIR spectrometer (Brucker Equinox 55 with MCT detector) - SPME-GC/MS (Perkin-Elmer Clarus 500)
480 L glass Wuppertal	480	1.4-39	3.7-5.7	Dimethylether ^c	- FTIR spectrometer (Thermo Nicolet 6700 with MCT detector)
ASC-IMT Lille Douai	300	0.065-0.65	1.6-10.2	Not used	- SMPS (TSI, DMA 3080 and CPC 3788)

(a) Experiments carried out under pseudo-first order conditions, with $[T2H]_0/[O_3]_0 \geq 10$

(b) Concentration of cyclohexane between 390 and 890 ppm (ASC-SAGE) and 1540 ppm (RASC-GSMA). One experiment in ASC was performed without cyclohexane.

(c) Used as OH tracer with concentrations between 15 and 22 ppm.

(d) Ozone was introduced continuously into RASC at a low flow rate.

Table 2. Kinetic results for T2H + O₃ in ASC and LFR. Uncertainties correspond to 2σ.

Reactor type	[T2H] ₀ (ppm)	[O ₃] ₀ (ppm)	Method	k (× 10 ¹⁸ cm ³ molecule ⁻¹ s ⁻¹)	Reference
Flow reactor	6.5-25	0.555	Absolute, T2H in excess	1.52 ± 0.19	This work
Chamber	1	0.2	Relative	2.00 ± 1.00	[20]
Chamber	2.34-3.5	0.073-0.114	Absolute, T2H in excess	1.28 ± 0.28	[23] ^a
Chamber	0.81-24	40-200	Absolute, O ₃ in excess	1.37 ± 0.03	[22] ^a

^aNot specified if 1σ or 2σ.

Table 3. Product formation yields of the ozonolysis of T2H from this work and comparison with literature data.

Presence of OH scavenger	Identified products	Yield (%)	References
No scavenger	Glyoxal	48 ± 10	This work (480-L)
	Butanal	33 ± 7	
	Acetaldehyde	Not quantified	
	Propanal	Not quantified	
Scavenger (Cyclohexane)	Glyoxal	59 ± 15	This work (RASC)
	Butanal	36 ± 9	
	Acetaldehyde	10 ± 3	
	Propanal	19 ± 5	
	2-hydroxybutanal	18 ± 6 ^a	
Scavenger (Cyclohexane)	Glyoxal	52.7 ± 5.5	[23]
	Butanal	55.9 ± 3.7	
	Acetaldehyde	10.9 ± 2	
	Propanal	6.7 ± 0.8	
	2-oxobutanal or 2-hydroxybutanal ^b	7.4 ± 0.6	

a: average of IR and GC analysis

b: Grosjean et al.^[23] were not able to distinguish between the two carbonyls (see text).

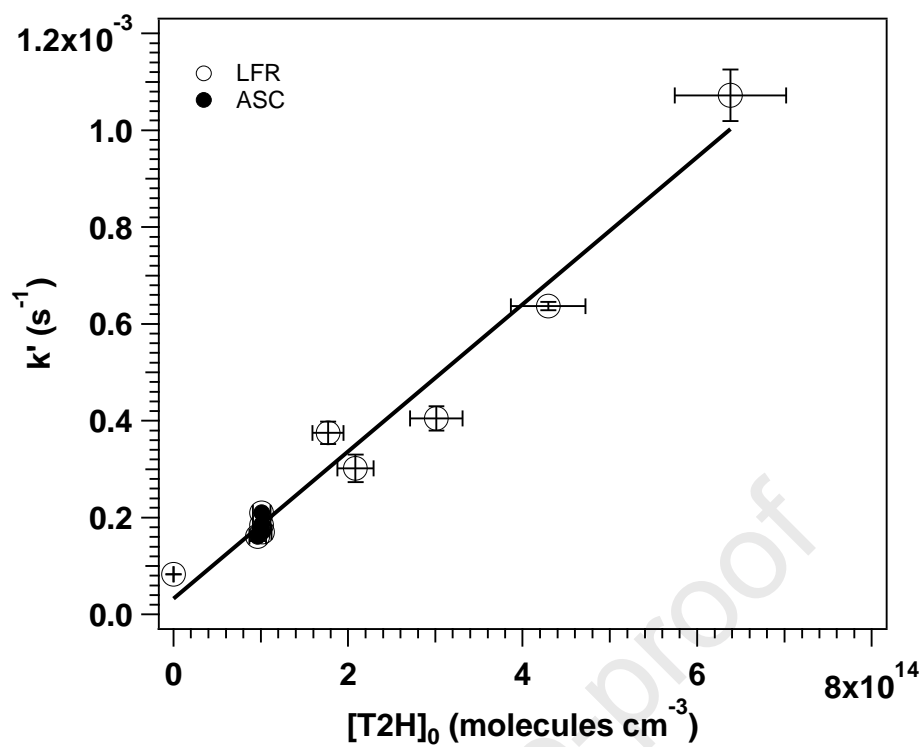
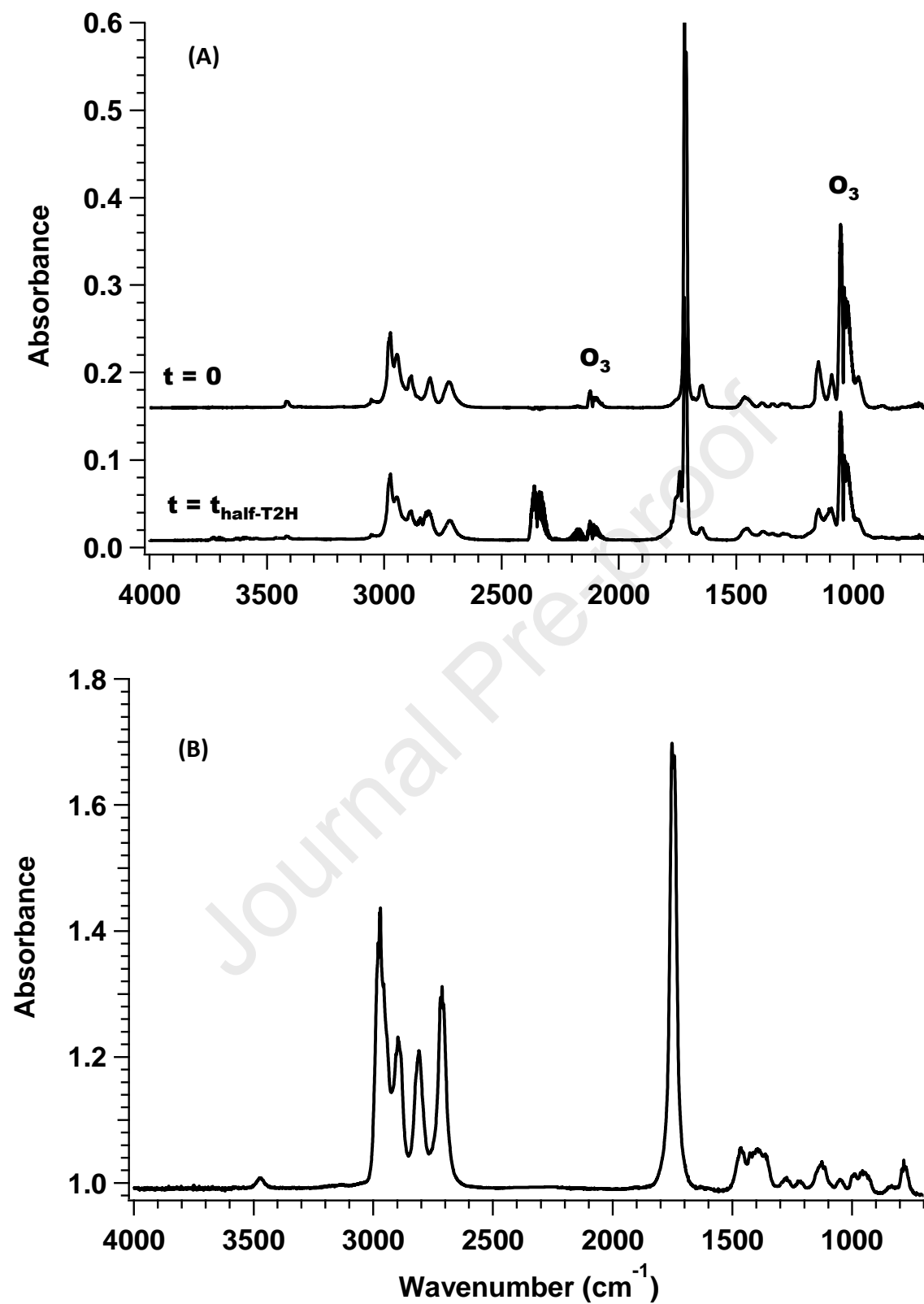
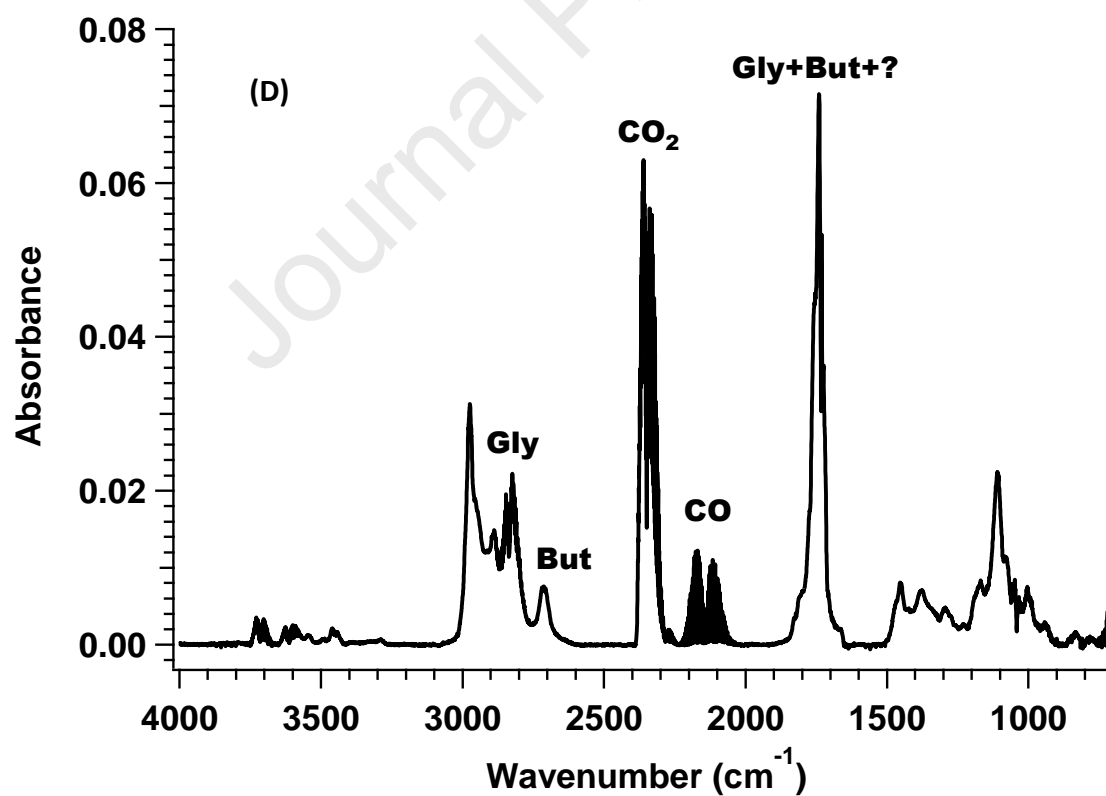
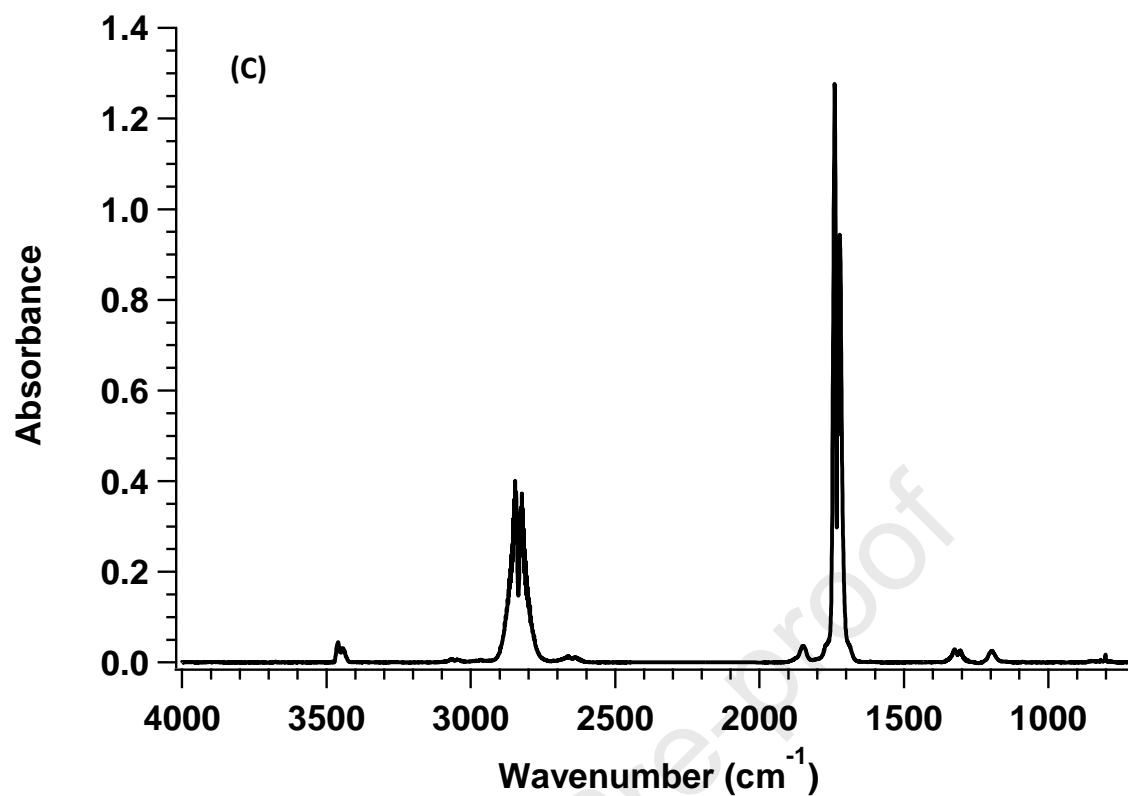


Figure 1. Plot of k' versus the initial concentration of T2H at room temperature performed in LFR (open symbols) and in ASC (filled symbols). The regression fit was carried out on both LFR and ASC data.





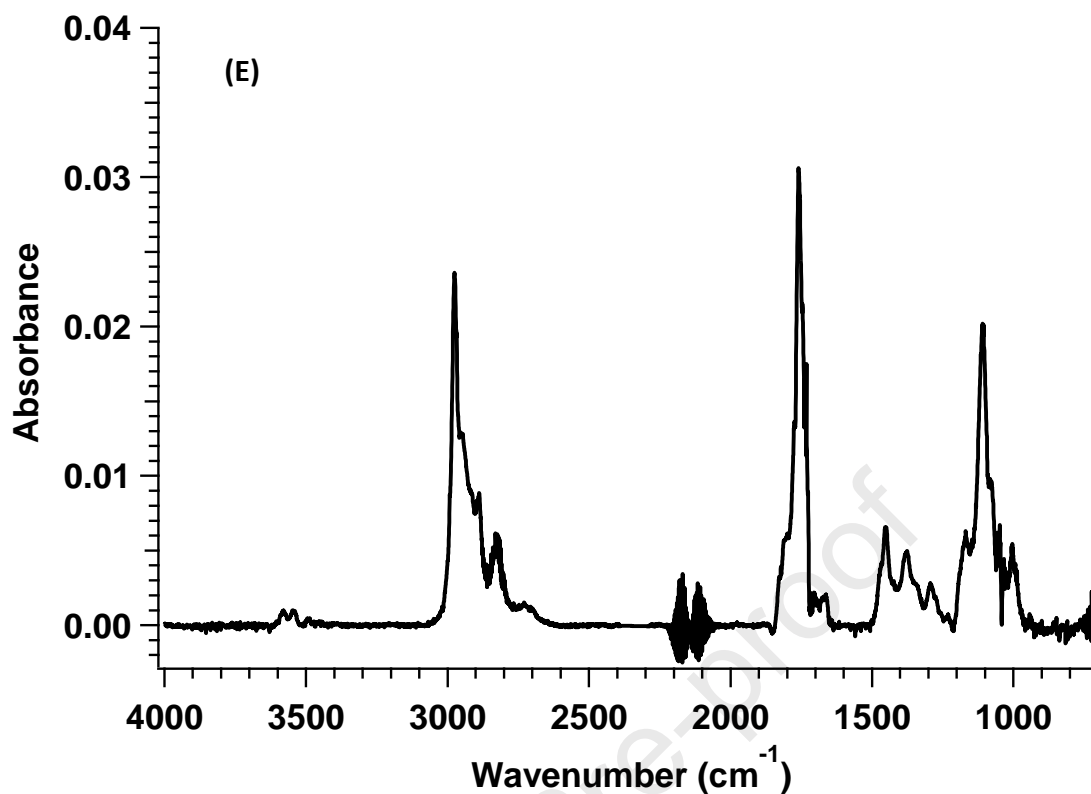


Figure 2. IR spectra obtained in the 480 L reactor. From bottom to top: Panel A shows the IR spectrum at $t = 0$ (O_3 bands are annotated; the other bands correspond to T2H) and after 50% T2H has reacted. Panels B and C show the reference spectra of butanal and glyoxal, respectively. Panel D displays the residual IR spectrum after removing T2H and O_3 (where Gly and But represent glyoxal and butanal, respectively). Panel E corresponds to the residual after removing butanal and glyoxal.

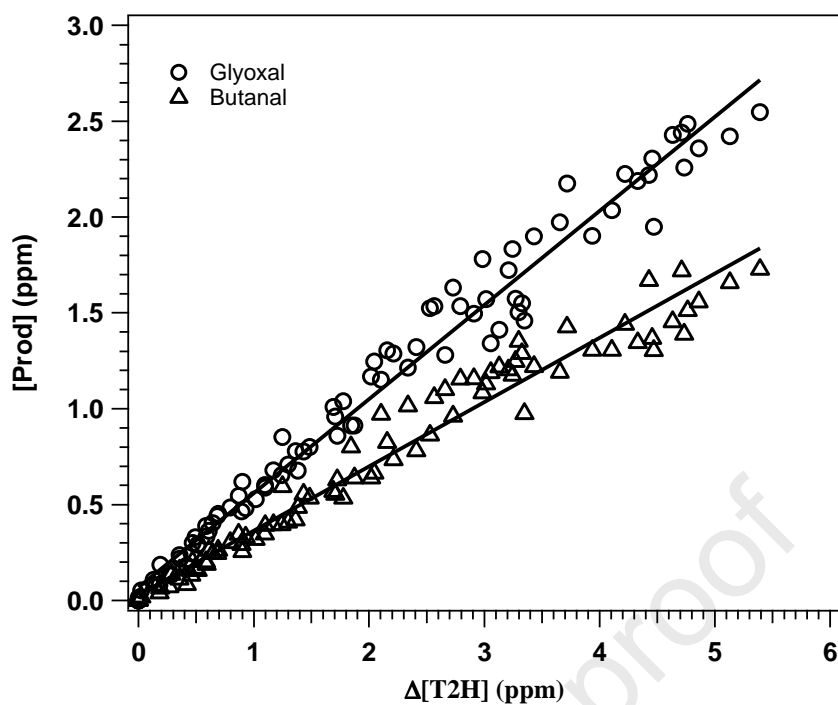


Figure 3. Plots of the concentrations of the glyoxal (○) and butanal (△) as a function of reacted T2H (FTIR analysis) obtained in the 480-L chamber (without OH scavenger)

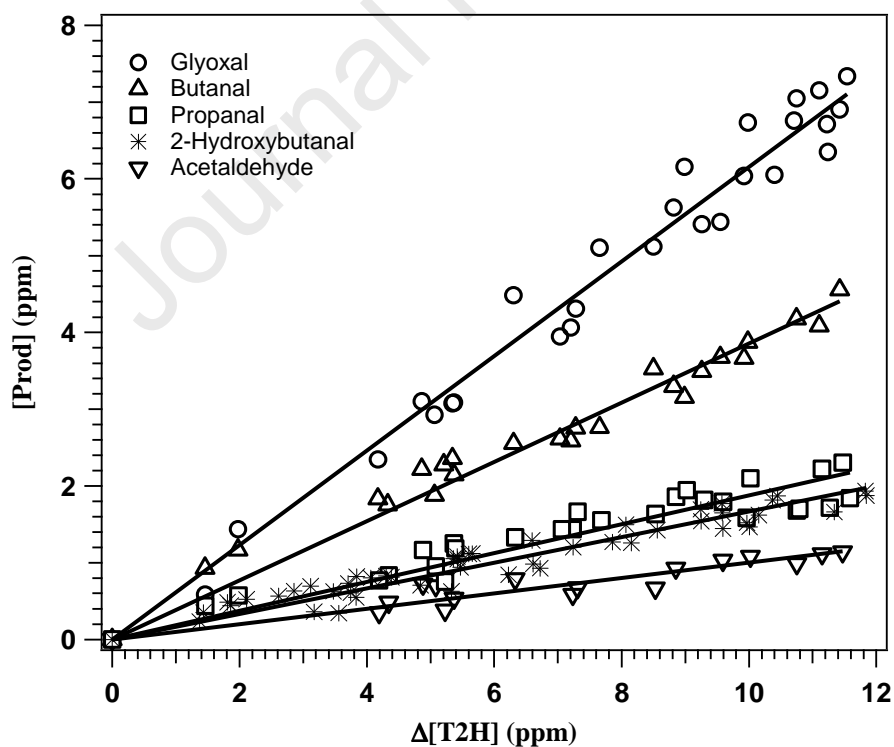


Figure 4. Plots of the concentrations of all the reaction products (GC-MS analysis) as a function of reacted T2H obtained in RASC (with OH scavenger)

Journal Pre-proof

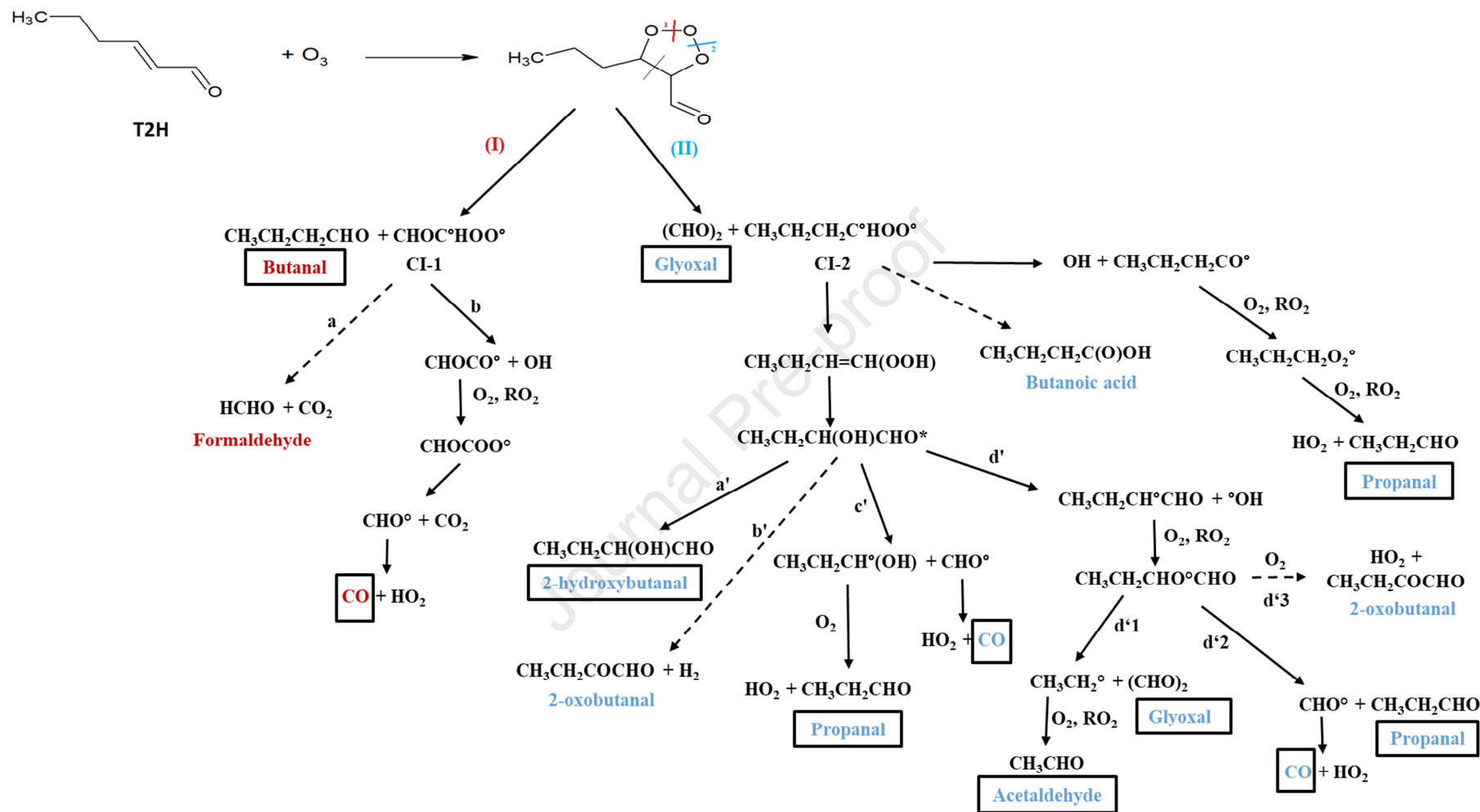


Figure 5. Proposed mechanistic scheme for the ozonolysis of T2H; framed products correspond to those identified in FTIR and GC/MS with and without an OH scavenger. Products from channel (I) are in red; products from channel (II) are in blue. Dashed arrows indicate reaction pathways that are negligible or not confirmed by the present results.

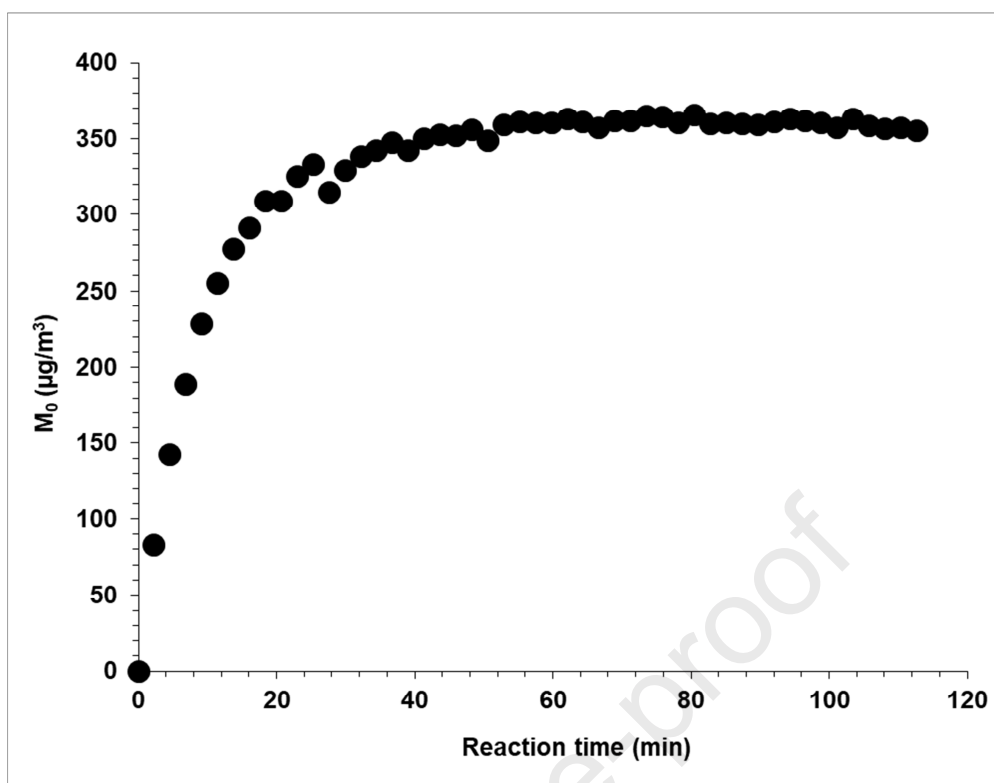


Figure 6. SOA formation as a function of time for T2H in ASC chamber (with $[\text{T2H}]_0 = 3.8$ ppm and $[\text{O}_3]_0 = 390$ ppb).

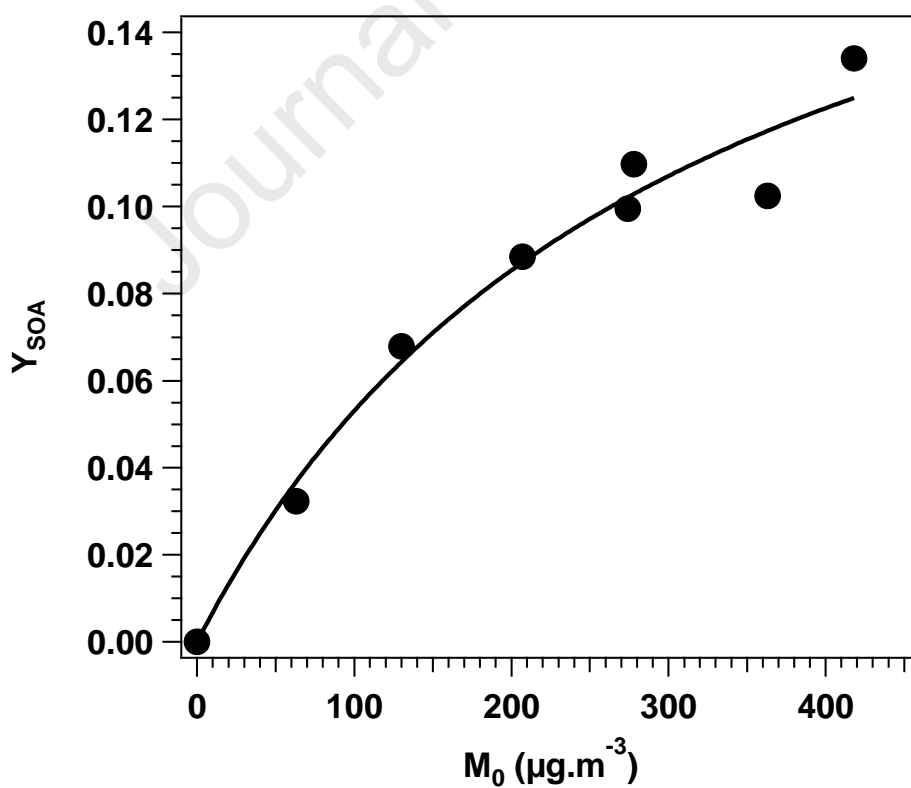


Figure 7. SOA formation yields Y_{SOA} vs. aerosol mass concentrations for T2H in ASC. The fit is carried out using Odum's one-product model (Eq. 5).

- Trans-2-hexenal ozonolysis kinetics and products investigated
- A reaction mechanism is proposed.
- First secondary organic aerosol investigation

Journal Pre-proof

Declaration of interests

The authors declare that they have no known competing financial interests or personal relationships that could have appeared to influence the work reported in this paper.

The authors declare the following financial interests/personal relationships which may be considered as potential competing interests:

Journal Pre-proof